Inorganic Chemistry

Article

pubs.acs.org/IC

Color-Tunable Emission and Energy Transfer in $Ca_3Gd_7(PO_4)(SiO_4)_5O_2$: $Ce^{3+}/Tb^{3+}/Mn^{2+}$ Phosphors

Yang Zhang,[†,‡] Guogang Li,[†,‡] Dongling Geng,[†,‡] Mengmeng Shang,[†,‡] Chong Peng,[†,‡] and Jun Lin*[,†]

[†]State Key Laboratory of Rare Earth Resource Utilization, Changchun Institute of Applied Chemistry, Chinese Academy of Sciences, Changchun 130022, People's Republic of China

[‡]University of the Chinese Academy of Sciences, Beijing 100049, People's Republic of China

Supporting Information

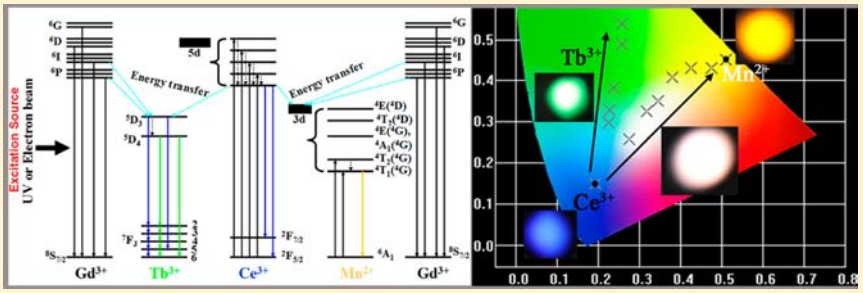

ABSTRACT: Ce^{3+}-, Tb^{3+}-, and Mn^{2+}-activated $Ca_3Gd_7(PO_4)(SiO_4)_5O_2$ (CGPS) silicate−phosphate oxyapatite phosphors have been prepared via conventional solid-state reaction processes. The Ce^{3+} emission at different lattice sites has been identified and discussed. The dual energy transfer of $Ce^{3+} \rightarrow Tb^{3+}$ and $Ce^{3+} \rightarrow Mn^{2+}$ has been investigated. The energy transfer from Ce^{3+} to Mn^{2+} in CGPS phosphors has been demonstrated to be a resonant type via a dipole−quadrupole mechanism, and the critical distances (R_C) for Ce^{3+} to Mn^{2+} calculated by the concentration quenching and spectral overlap methods are 9.71 and 9.15 Å, respectively. A color-tunable emission in CGPS phosphors can be realized by $Ce^{3+} \rightarrow Tb^{3+}$ or $Ce^{3+} \rightarrow Mn^{2+}$ energy transfer. CGPS:0.05Ce^{3+}/ 0.15Tb^{3+} shows the optimum green emission. Meanwhile, white cathodoluminescence (CL) has been realized in a single-phased $Ca_3Gd_7(PO_4)(SiO_4)_5O_2$ host by codoping with Ce^{3+} and Mn^{2+} with CIE (0.322, 0.326). Furthermore, the CL properties of CGPS:$Ce^{3+}/Tb^{3+}/Mn^{2+}$ phosphors, including the dependence of the CL intensity on the accelerating voltage and filament current, the decay behavior of the CL intensity under electron bombardment, and the stability of the CIE chromaticity coordinates, have been investigated in detail. Because of the good CL properties and good CIE chromaticity coordinates, the as-prepared phosphors have potential application in field emission display devices.

1. INTRODUCTION

Recently, the development of phosphors arouses a fast-growing interest because of a wide range of applications: white-light-emitting diodes, cathode ray tubes (CRTs), vacuum fluorescent displays, plasma display panels, and X-ray imaging scintillators, and field emission displays (FEDs).[1−6] Especially, FEDs have been considered as one of the most promising next-generation flat-panel displays because of their potential to provide displays with thin panels, self-emission, wide viewing, quick response time, high brightness, high contrast ratio, light weight, and low power consumption.[5] For FEDs, phosphors must be operated at significantly lower excitation voltages (≤5 kV) and higher current densities (10−100 μA cm^{-2}) than CRTs.[7,8] Thus, one of the most important factors is to develop highly efficient phosphors at low voltages, higher resistance to current saturation, and good chemical durability. Many commercially sulfide-based phosphors, such as $Y_2O_2S:Eu^{3+}$, $Gd_2O_2S:Tb^{3+}$, $SrGa_2S_4:Eu^{3+}$, Zn(Cd)S:Cu,Al, ZnS:Ag,Cl, etc., have been widely used as possible low-voltage phosphors.[9−11] Unfortunately, because of the poor stability, sulfide-based phosphors often degrade under electron bombardment, which contaminates the emission tips and shortens the device lifetime. On the other hand, sulfide-based phosphors are not friendly to the environment.[12] Thus, it is urgent for us to develop some novel phosphors with better stability and higher efficiency. During the past decade, extensive research has been carried out on oxide-based phosphors because of their superior color richness and good chemical and thermal stability compared to those of nonoxide materials, e.g., sulfides, doped with the d or s series elements.[13−15]

Because of the abundant emission colors based on their 4f → 4f or 5d → 4f transitions, rare-earth (RE) ions have been playing an irreplaceable role in modern lighting and display fields.[16,17] Especially, energy transfer between RE ions plays an important role in the development of color-tunable single-phased phosphors from both theoretical and practical points of view.[18−20] As we all know, the Ce^{3+} ion with the $4f^1$ configuration may act as a highly efficient emission center because 4f → 5d transitions of the Ce^{3+} ion are allowed by the

Received: July 17, 2012
Published: October 17, 2012

   dx.doi.org/10.1021/ic3015578 | Inorg. Chem. 2012, 51, 11655−11664

Laporte parity selection rules.[18,21] In addition, the Ce^{3+} ion can also act as an efficient sensitizer to enhance the emission of coactivators by transferring part of its excitation energy to them, such as Tb^{3+} and Mn^{2+}.[22−24] So far, $Ce^{3+} \rightarrow Tb^{3+}$ or $Ce^{3+} \rightarrow Mn^{2+}$ energy transfer has been investigated; i.e., Ce^{3+} ions serving as effective sensitizer ions not only help Tb^{3+} and Mn^{2+} ions to emit efficiently but also tune their emission colors from blue to green and from blue to yellow/red, respectively.[25] Consequently, it is meaningful to develop some single-phased phosphors with multicolor-tunable emission via energy transfer for application in FEDs.

Apatites contain a large number of inorganic compounds with the general formula $M_{10}(EO_4)_6X_2$, where M is a univalent to trivalent cation (Ca^{2+}, Sr^{2+}, Ba^{2+}, Cd^{3+}, Eu^{3+}, Y^{3+}, La^{3+}, Na^{+}, K^{+}, etc.), E is a tetravalent to hexavalent element (P^{5+}, V^{5+}, As^{5+}, Si^{4+}, Ge^{4+}, S^{6+}, Cr^{6+}, etc.), and X represents anions OH^{-}, F^{-}, Cl^{-}, Br^{-}, I^{-}, and O^{2-}.[26−28] Furthermore, silicate−phosphates resulting from the substitution of (Gd^{3+}, SiO_4^{4-}) for (Ca^{2+}, PO_4^{3-}) show some interesting properties.[29,30] It is well-known that the compounds with oxyapatite structure (space group $P6_3/m$) have been effectively used as host lattices for luminescent materials because of their applications in the medical field and solid-state lighting industry.[31] The silicate−phosphates host lattice contains two cationic sites, that is, 9-fold-coordinated 4f sites with C_3 point symmetry and 7-fold-coordinated 6h sites with C_s point symmetry. Both sites are suitable and easily accommodate a great variety of RE^{3+} ions.[32] To the best of our knowledge, there are no reports about the detailed photoluminescence (PL) properties of Ce^{3+}, Tb^{3+}, and Mn^{2+} and the sensitization effect of $Ce^{3+} \rightarrow Tb^{3+}$ or $Ce^{3+} \rightarrow Mn^{2+}$ luminescence in the $Ca_3Gd_7(PO_4)(SiO_4)_5O_2$ (CGPS) host lattice. Moreover, the cathodoluminescence (CL) properties of $Ce^{3+}/Tb^{3+}/Mn^{2+}$-coactivated CGPS phosphors have not been reported. Accordingly, in this paper, we reported the synthesis of CGPS:$Ce^{3+}/Tb^{3+}/Mn^{2+}$ phosphors via the solid-state reaction process, and a systematic study on the PL and CL properties of these phosphors has been carried out in detail. It is found that they have potential application in FEDs.

2. EXPERIMENTAL SECTION

2.1. Materials. The initial rare-earth oxides, including CeO_2 (99.999%), Tb_4O_7 (99.999%), and Gd_2O_3 (99.999%), were purchased from Science and Technology Parent Company of Changchun Institute of Applied Chemistry, and $CaCO_3$ (Aldrich, 99.99%), SiO_2 (Aldrich, 99.99%), $MnCO_3$ (Aldrich, 99.99%), and $(NH_4)_2HPO_4$ were purchased from Beijing Chemical Company. All chemicals were used directly without further purification.

2.2. Preparation. A series of CGPS:xCe^{3+},yTb^{3+},zMn^{2+} (abbreviated as CGPS:xCe,yTb,zMn, where x, y, and z are mole percent) powder samples were prepared by the conventional solid-state reaction process. The doping concentrations of Ce^{3+}, Tb^{3+}, and Mn^{2+} were chosen as 1−10% and 5−25% of Gd^{3+} and 1−20 mol % of Ca^{2+} in CGPS, respectively. Typically, the stoichiometric amounts of $CaCO_3$, Gd_2O_3, $(NH_4)_2HPO_4$, SiO_2, CeO_2, Tb_4O_7, and $MnCO_3$ with purity higher than 99.99% were mixed in an agate mortar by the addition of ethanol and then adequately triturated for good mixing. The dried powders were obtained after baking in an oven at 80 °C for 20 min. Then the mixtures were calcined at 1400 °C for 3 h in a reducing atmosphere of H_2 (10%) and N_2 (90%).

2.3. Characterization. The X-ray diffraction (XRD) patterns were performed on a D8 Focus diffractometer at a scanning rate of 10° min^{-1} in the 2θ range from 20° to 70° with graphite-monochromatized Cu Kα radiation (λ = 0.15405 nm). The PL measurements were recorded with a Hitachi F-7000 spectrophotometer equipped with a 150 W xenon lamp as the excitation source. The CL measurements were conducted in an ultrahigh-vacuum chamber (<10^{-8} Torr), where the phosphors were excited by an electron beam at a voltage range of 2−6 kV with different filament currents of 80−96 mA, and the spectra were recorded using an F-7000 spectrophotometer. The luminescence decay curves were obtained from a Lecroy Wave Runner 6100 digital osilloscope (1 GHz) using a tunable laser (pulse width = 4 ns; gate = 50 ns) as the excitation source (Continuum Sunlite OPO). All of the measurements were performed at room temperature.

3. RESULTS AND DISCUSSION

3.1. Structure. The composition and phase purity of the as-prepared powder samples were first examined by XRD. The XRD patterns of CGPS:$Ce^{3+}/Tb^{3+}/Mn^{2+}$, together with the Joint Committee on Powder Diffraction Standards (JCPDS) card no. 29-0326, are shown in Figure 1. All of the diffraction peaks of these samples can be exactly assigned to the pure hexagonal phase of CGPS [space group $P6_3/m$ (No. 176)]. The XRD patterns for different Ce^{3+}, Tb^{3+}, and Mn^{2+} concentrations of doped CGPS samples are similar to the above results in Figure 1. No obvious shifting of the peaks or other impurity phases can be detected at the current doping level (Figures S1 and S2 in the Supporting Information, SI). The silicate−phosphate CGPS is isostructural to natural oxyapatite $Ca_{10}(PO_4)_6F_2$, which has a hexagonal space group $P6_3/m$ and cell parameters of a = 9.408 Å, c = 6.891 Å, V = 528.21 Å^3, and Z = 1. The crystal structure of CGPS, shown in Figure S3 in the SI, also indicates that the surrounding nine O atoms of the cation located at the 4f site (C_3) form a tetrakaidecahedron, and these tetrakaidecahedra are connected by tetrahedral PO_4/SiO_4 groups, while the cations located at the 6h site (C_s) form decahedra with the surrounding seven O atoms, and these decahedra connect each other through the sharing plane, edge, and vertex. Finally, the tetrakaidecahedron and decahedron are connected through tetrahedral PO_4/SiO_4 groups and through the sharing plane, edge, and vertex. As suggested by Blasse,[31,33] the most prominent structural characteristics of the CGPS crystal structure are the two Gd^{3+} sites, which are the 4f (C_3) site with nine-coordination [Gd^{3+}(I)] and the 6h (C_s) site with seven-coordination [Gd^{3+}(II)], while Ca^{2+} only occupies the 4f (C_3) site with nine-coordination. Therefore, on the basis of the effective ionic radii and charge balance, we suggest that Ce^{3+}/Tb^{3+} ions prefer to occupy Gd^{3+} sites while Mn^{2+} ions replace Ca^{2+} ions more easily.[20,34] In addition, the structure parameters

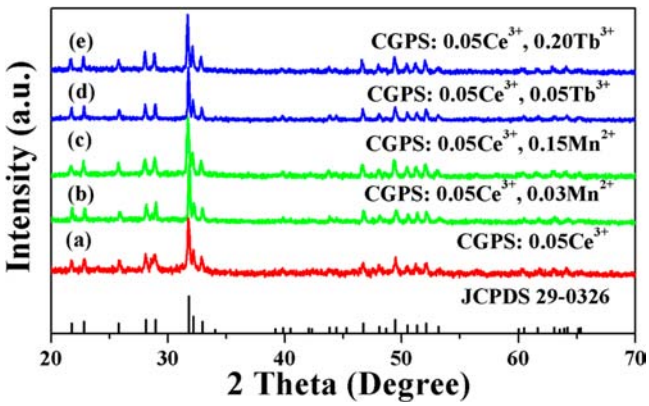

Figure 1. XRD patterns of $Ce^{3+}/Tb^{3+}/Mn^{2+}$-doped CGPS samples annealed at 1400 °C for 3 h in H_2/N_2 (10%/90%) and the standard data of CGPS (JCPDS card no. 29-0326).

dx.doi.org/10.1021/ic3015578 | Inorg. Chem. 2012, 51, 11655−11664

and ionic radii for given coordination numbers (CNs) have been summarized and are shown in Table 1.

Table 1. Structure Parameters of CGPS and Ionic Radii (Å) for Given CNs of Gd^{3+}, Ce^{3+}, Tb^{3+}, Ca^{2+}, and Mn^{2+} Ions

				ionic radius (Å)	
ion	space group	sites	symmetry	CN = 9	CN = 7
Gd^{3+}	hexagonal $P6_3/m$ (No. 176)	4f/6h	C_3/C_s	1.107	1.00
Ce^{3+}				1.196	1.07
Tb^{3+}				1.095	0.98
Ca^{2+}		4f	C_3	1.18	1.06
Mn^{2+}					0.90

3.2. PL Properties of CGPS:Ce^{3+}/Tb^{3+}. The emission and excitation spectra of CGPS:0.05Ce^{3+} are presented in Figure 2a.

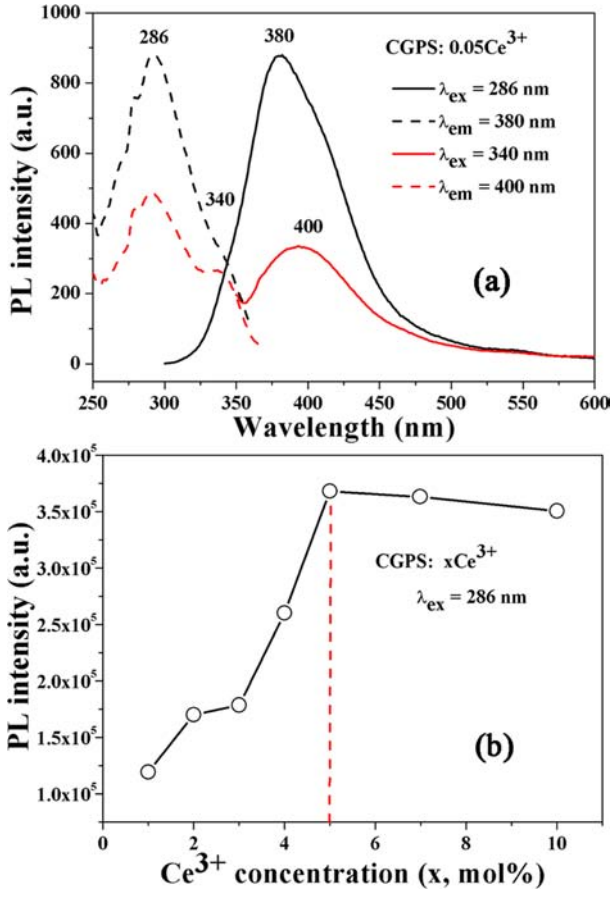

Figure 2. (a) Excitation and emission spectra of the CGPS:0.05Ce^{3+} sample. (b) PL intensity of CGPS:$x$$Ce^{3+}$ samples as a function of the Ce^{3+} doping concentration.

The Ce^{3+} singly doped sample exhibits a broad band that extends from 300 to 500 nm with a maximum at about 380 nm when excited by 286 nm UV light. However, the emission maximum of CGPS:0.05Ce^{3+} is red-shifted to 400 nm when using 340 nm UV light as the excitation source. It is well-known that the energy difference between transitions of the Ce^{3+} ions from the 5d excited state to the $^2F_{7/2}$ and $^2F_{5/2}$ ground states should be about 2000 cm^{-1}. However, the energy difference between 380 and 400 nm is about 1316 cm^{-1}, which is far from 2000 cm^{-1}. Thus, we speculated that there exist two types of Ce^{3+} luminescent centers in CGPS. This is related to the crystal structure of CGPS, which provides two different sites for the Gd^{3+} cations in it as discussed earlier, i.e., Gd^{3+}(I) located at the 4f (C_3) site and Gd^{3+}(II) at the 6h (C_s) site. Because of the large ionic radius (1.196 Å for CN = 9) and high charge (3+), it is easy for Ce^{3+} to occupy both 4f and 6h sites.[21,35] The major difference between the two sites is that the 6h site has a free O ion, which does not belong to any silicate group so that its binding strength is not saturated with respect to the 4f site.[21] In summary, the higher-energy emission band centered at 380 nm should involve the 5d → 4f transition of Ce^{3+} occupying the Gd^{3+}(I) site with nine-coordination, and the lower-energy emission band centered at 400 nm involves the 5d → 4f transition of Ce^{3+} occupying the Gd^{3+}(II) site with seven-coordination. The excitation spectrum can be classified in the same way, i.e., the 286 nm band to Ce^{3+} occupying Gd^{3+}(I) with the 4f (C_3) site and the 340 nm band to Ce^{3+} occupying Gd^{3+}(II) with the 6h (C_s) site. Figure 2b shows the PL intensity of Ce^{3+} as a function of its doping concentration (x) in CGPS:$x$$Ce^{3+}$ samples. First, the PL emission intensity of Ce^{3+} (λ_{ex} = 286 nm) increases with an increase of its concentration (x), reaching a maximum value at x = 0.05 and then decreasing with a further increase of its concentration (x) due to the concentration quenching effect.[36,37] Thus, the optimum doping concentration for Ce^{3+} ions is 5 mol % of Gd^{3+} in the CGPS host. The critical distance R_C between Ce^{3+} ions can be estimated using the equation given by Blasse:[38]

$$R_C \approx 2\left[\frac{3V}{4\pi X_C N}\right]^{1/3} \quad (1)$$

where V is the volume of the unit cell, N is the number of host cations in the unit cell, and X_C is the critical concentration of doped ions. For the CGPS host, N = 10 (N = 7 for Ce^{3+} ions), V = 528.21 $Å^3$, and X_C is 5% for Ce^{3+}; therefore, the critical distance (R_C) was calculated to be about 14.23 Å.

Owing to the high degeneracy of the Tb^{3+} levels involved in several transitions, it is difficult to derive information from the Tb^{3+} spectra on the nature of the Tb^{3+} center.[22] Generally, the Tb^{3+} ion is used as an activator in green phosphors, whose emission is mainly due to transitions of $^5D_3 \rightarrow {}^7F_J$ in the blue region and $^5D_4 \rightarrow {}^7F_J$ in the green region (J = 6, 5, 4, 3, 2) depending on its doping concentration.[15] Figure 3a shows excitation and emission spectra of the CGPS:0.02Tb^{3+} sample. The excitation spectrum shows a strong broad band (λ_{max} = 230 nm) with a shoulder at 276 nm, which are due to a spin-allowed $4f^8 \rightarrow 4f^7 5d$ (ΔS = 0) transition of Tb^{3+} and the $^8S \rightarrow {}^6I$ transitions of Gd^{3+} ions, respectively, indicating that there is an energy transfer from Gd^{3+} to Tb^{3+}.[39,40] Under 230 nm UV excitation, the emission spectra of the as-prepared CGPS:0.02Tb^{3+} consists of the $^5D_{3,4} \rightarrow {}^7F_J$ transitions of Tb^{3+}, as shown in Figure 3a (green line). In addition, under 276 nm UV excitation, there is a sharp peak at 313 nm from the $^6P_{7/2} \rightarrow {}^8S_{7/2}$ transition of Gd^{3+} besides the $^5D_{3,4} \rightarrow {}^7F_J$ transitions of Tb^{3+} (350−700 nm) in the emission spectra, which is more strong evidence for energy transfer from Gd^{3+} to Tb^{3+} in the CGPS host.

The Ce^{3+} ion is a well-known sensitizer for trivalent RE ion and transitional-metal ion luminescence, and the sensitizing effects depend strongly on the host lattices into which these ions are introduced. Energy transfer was expected to occur from Ce^{3+} to Tb^{3+} based on the significant spectral overlap between the emission band of Ce^{3+} and the Tb^{3+} excitation transitions in

dx.doi.org/10.1021/ic3015578 | Inorg. Chem. 2012, 51, 11655−11664

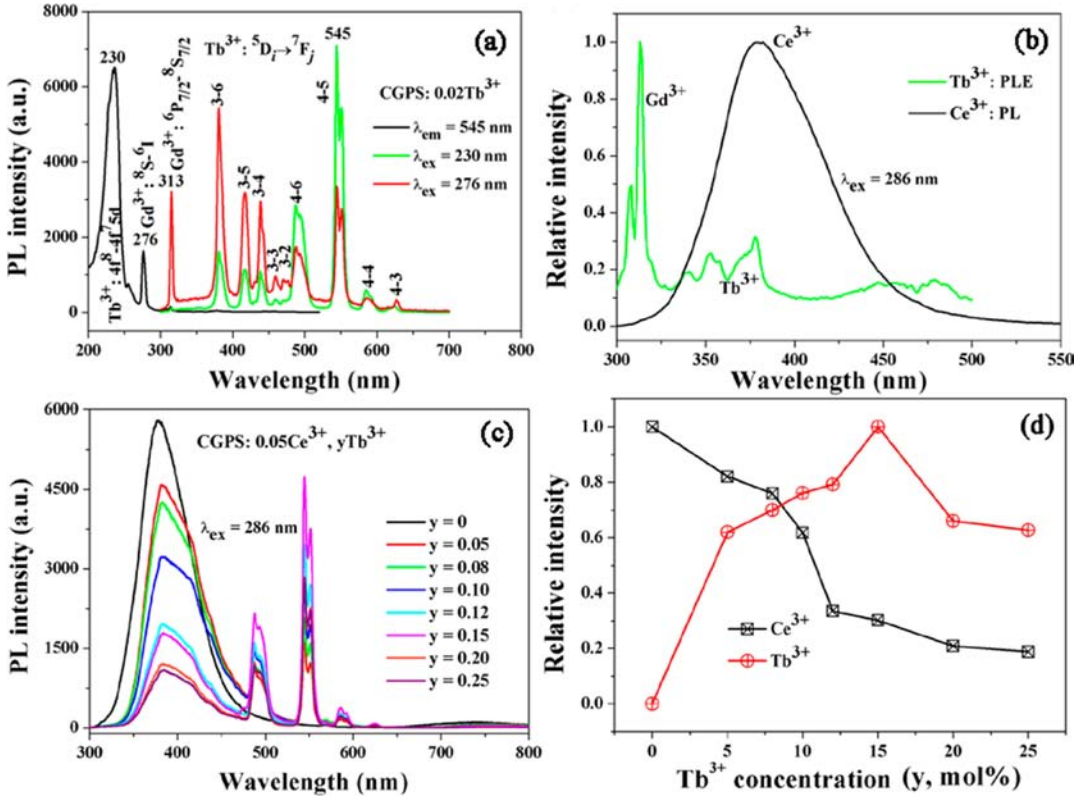

Figure 3. (a) Excitation and emission spectra of the CGPS:0.02Tb^{3+} sample. (b) Spectral overlap between the PL spectrum of CGPS:0.05Ce^{3+} (black line) and the PLE spectrum of CGPS:0.02Tb^{3+} (green line). Variation of (c) the PL spectra and (d) the emission intensity of Ce^{3+} and Tb^{3+} in the CGPS:Ce^{3+},Tb^{3+} system with changing Tb^{3+} and fixed Ce^{3+} doping concentrations.

the range 350−450 nm, as shown in Figure 3b. The excitation spectrum monitored with the Tb^{3+} $^5D_4 \rightarrow {}^7F_5$ transition (545 nm) of the CGPS:0.05Ce^{3+},0.15Tb^{3+} sample (Figure S4 in the SI) consists of excitation bands of the Ce^{3+} and Tb^{3+} ions. The first band (200−250 nm) is due to absorption of the Tb^{3+} $4f^8 \rightarrow 4f^7 5d$ transition, and the latter (250−350 nm) is caused by the Ce^{3+} 4f → 5d transition. The presence of the Ce^{3+} absorption band suggests that the energy transfer process from Ce^{3+} to Tb^{3+} exists. Parts c and d of Figure 3 show variation of the PL spectra and emission intensity of Ce^{3+} and Tb^{3+} in the CGPS:0.05Ce^{3+},*y*Tb^{3+} system with changing Tb^{3+} doping concentration, respectively. Although the concentration of Ce^{3+} was fixed at 5%, the emission intensity of Ce^{3+} decreased with increasing Tb^{3+} concentration. The energy-transfer efficiency (η_T) from the Ce^{3+} to Tb^{3+} ions in CGPS:0.05Ce^{3+},*y*Tb^{3+} was calculated using the formula[41]

$$\eta_T = 1 - \frac{I_S}{I_{S0}} \quad (2)$$

where η_T is the energy-transfer efficiency and I_{S0} and I_S are the luminescence intensity of a sensitizer (Ce^{3+}) in the absence and presence of an activator (Tb^{3+}), respectively. The η_T value of CGPS:0.05Ce^{3+},*y*Tb^{3+} could be obtained as a function of *y* and is presented in Figure 4, in which the maximum energy-transfer efficiency can reach 81% when using 286 nm UV as the monitoring wavelength. All of these results indicate the efficient energy transfer from Ce^{3+} to Tb^{3+}. In view of the $Ce^{3+} \rightarrow Tb^{3+}$ transition in the CGPS host, Ce^{3+} ions can strongly absorb UV light from the ground state ($^2F_{5/2}$) to the excited state and then efficiently transfer the energy to the $^5D_3$ level of Tb^{3+} ions; subsequently, the $^5D_3$ level gives its characteristic transitions or

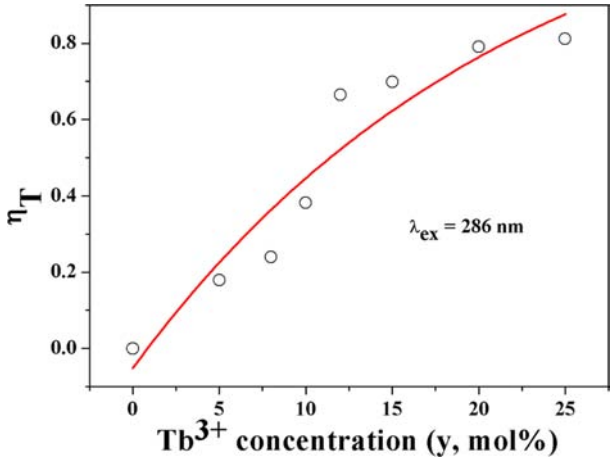

Figure 4. Energy-transfer efficiency from Ce^{3+} to Tb^{3+} in CGPS:0.05Ce^{3+},*y*Tb^{3+} (0−0.25) samples (λ_{ex} = 286 nm).

continues to transfer the energy to the $^5D_4$ level via cross-relaxation, as shown in Figure 5. In addition, we could tune the emission color from blue to green through energy transfer, as shown in Table 2. There are two main aspects responsible for the resonant energy-transfer mechanism: one is exchange interaction, and the other is multipolar interaction.[42] It is known that if energy transfer results from exchange interaction, the critical distance between the sensitizer and activator should be shorter than 4 Å. The critical distance R_C for energy transfer from the Ce^{3+} to Tb^{3+} ions could be calculated using eq 1. Here, *X* is the total concentration of Ce^{3+} and Tb^{3+} ions, and the critical concentration (X_C) is that at which the

dx.doi.org/10.1021/ic3015578 | Inorg. Chem. 2012, 51, 11655−11664

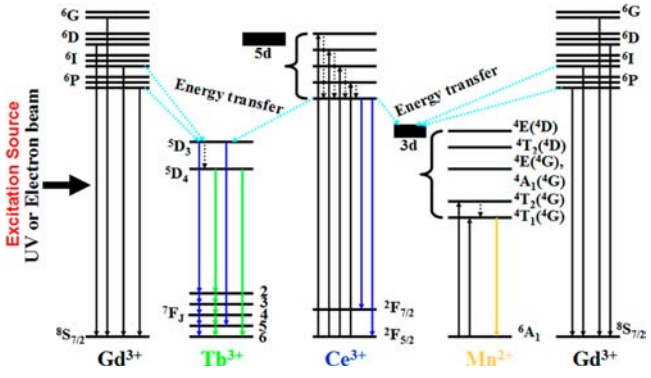

Figure 5. Illustration of the energy-transfer mechanism for Ce^{3+}/Tb^{3+} and Ce^{3+}/Mn^{2+} pairs in the CGPS host.

luminescence intensity of the sensitizer (Ce^{3+}) is half that in the sample in the absence of an activator (Tb^{3+}); i.e., X_C occurs when $\eta_T = 0.5$. Therefore, the critical distance (R_C) between Ce^{3+} and Tb^{3+} ions calculated by the concentration quenching method (eq 1) is 9.66 Å. The radiative emission from Ce^{3+} prevails when $R_{Ce-Tb} > R_C$ and energy transfer from Ce^{3+} to Tb^{3+} dominates when $R_{Ce-Tb} < R_C$. This value is much longer than 4 Å, indicating little possibility of energy transfer via the exchange interaction mechanism. Thus, energy transfer between the Ce^{3+} and Tb^{3+} ions mainly takes place via electric multipolar interactions. According to Dexter's energy-transfer expressions of multipolar interaction and Reisfeld's approximation, the following relation can be given:[36,42]

$$\frac{\eta_0}{\eta} \propto C^{n/3} \tag{3}$$

where η_0 and η are the luminescence quantum efficiency of Ce^{3+} in the absence and presence of Tb^{3+}, C is the total content of Ce^{3+} and Tb^{3+}, n = 6, 8, and 10 corresponding to dipole−dipole, dipole−quadrupole, and quadrupole−quadrupole interactions, respectively. The value η_0/η can be approximately estimated by the ratio of related luminescence intensities as[20,43,44]

$$\frac{I_{S0}}{I_S} \propto C^{n/3} \tag{4}$$

where I_{S0} is the intrinsic luminescence intensity of Ce^{3+} and I_S is the luminescence intensity of Ce^{3+} in the presence of Tb^{3+}. The $I_{S0}/I_S - C_{Ce+Tb}{}^{n/3}$ plots are further illustrated in Figure 6a−c, and the relationships are observed when n = 6, 8, and 10. Only when n = 8, it shows a linear relation, implying that the dipole−quadrupole interaction should be mainly responsible for energy transfer from the Ce^{3+} to Tb^{3+} ions, which is consistent with a previous report.[40]

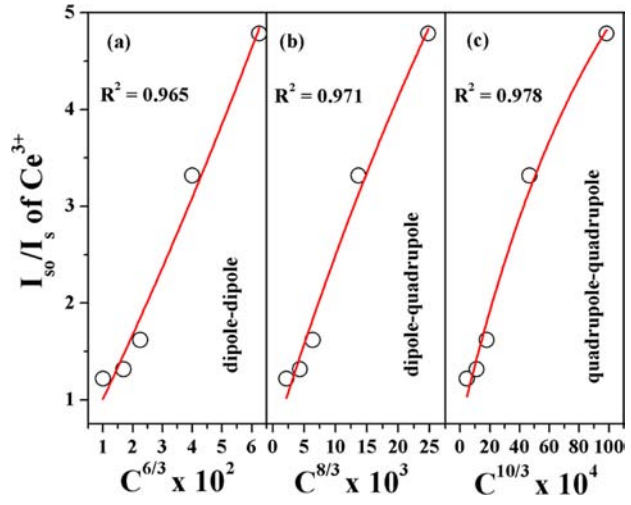

Figure 6. Dependence of I_{S0}/I_S of Ce^{3+} on (a) $C_{Ce+Tb}{}^{6/3}$, (b) $C_{Ce+Tb}{}^{8/3}$, and (c) $C_{Ce+Tb}{}^{10/3}$.

3.3. PL Properties of CGPS:Ce^{3+}/Mn^{2+}. The Mn^{2+} ion with $3d^5$ electronic configuration generally shows a broad emission band (500−700 nm) because of the $^4T_1 \rightarrow {}^6A_1$ transition within the 3d shell, in which the electrons are strongly coupled to lattice vibration and affected by the crystal-field strength and site symmetry. If Mn^{2+} ions lie in the weak crystal-field condition, the splitting of the excited-state d energy levels will be small, resulting in Mn^{2+} emission with higher energy as a green emission; if it is in strong crystal-field condition, a yellow/red emission is usually obtained.[35] Figure 7a shows the excitation and emission spectra of the CGPS:0.09Mn^{2+} sample. The broad emission band centered at 575 nm is attributed to the spin-forbidden $^4T_1(4G) \rightarrow {}^6A_1(6S)$ transition of Mn^{2+} occupying the Ca^{2+} site with nine-coordination. The excitation spectrum consists of several weak bands centered at 293, 341, and 376 nm corresponding to the transitions from $^6A_1(6S)$ to $^4T_1(^4P)$, $^4E(^4D)$, and $^4T_2(^4D)$ of Mn^{2+}, respectively, while the strong band centered at 276 nm is assigned to the $^8S \rightarrow {}^6I$ transition of Gd^{3+}.[19,39,43] Because these transitions of Mn^{2+} are spin- and parity-forbidden, it is difficult to pump and the emission intensity is very weak, as shown in Figure 7a (red line) monitored at 376 nm. As is shown in Figure 5, Gd^{3+} ions can strongly absorb UV light from the ground state ($^8S_{7/2}$) to the excited state and then efficiently transfer the energy to Mn^{2+} ions. Because of the energy migration process $Gd^{3+} \rightarrow (Gd^{3+})_n \rightarrow Mn^{2+}$ in CGPS, the emission intensity monitoring at 276 nm is much higher than that at 376 nm with the same maximum emission at 575 nm, which is consistent with the previous report.[45] Similarly, energy transfer was expected to occur from Ce^{3+} to Mn^{2+} based on the

Table 2. Chromaticity Coordinates (x, y) of CGPS:$Ce^{3+}/Mn^{2+}/Tb^{3+}$ Samples under UV Excitation (λ_{ex} = 286 nm)

sample	CIE coordinates (x, y)	sample	CIE coordinates (x, y)
CGPS:0.05Ce^{3+}	(0.166, 0.093)	CGPS:0.09Mn^{2+}	(0.519, 0.438)
CGPS:0.05Ce^{3+},0.05Tb^{3+}	(0.179, 0.144)	CGPS:0.05Ce^{3+},0.01Mn^{2+}	(0.312, 0.261)
CGPS:0.05Ce^{3+},0.08Tb^{3+}	(0.186, 0.172)	CGPS:0.05Ce^{3+},0.03Mn^{2+}	(0.366, 0.308)
CGPS:0.05Ce^{3+},0.10Tb^{3+}	(0.186, 0.200)	CGPS:0.05Ce^{3+},0.05Mn^{2+}	(0.393, 0.321)
CGPS:0.05Ce^{3+},0.12Tb^{3+}	(0.209, 0.318)	CGPS:0.05Ce^{3+},0.07Mn^{2+}	(0.404, 0.350)
CGPS:0.05Ce^{3+},0.15Tb^{3+}	(0.212, 0.329)	CGPS:0.05Ce^{3+},0.09Mn^{2+}	(0.437, 0.369)
CGPS:0.05Ce^{3+},0.20Tb^{3+}	(0.222, 0.382)	CGPS:0.05Ce^{3+},0.15Mn^{2+}	(0.466, 0.399)
CGPS:0.05Ce^{3+},0.25Tb^{3+}	(0.231, 0.431)	CGPS:0.05Ce^{3+},0.20Mn^{2+}	(0.481, 0.420)

dx.doi.org/10.1021/ic3015578 | Inorg. Chem. 2012, 51, 11655−11664

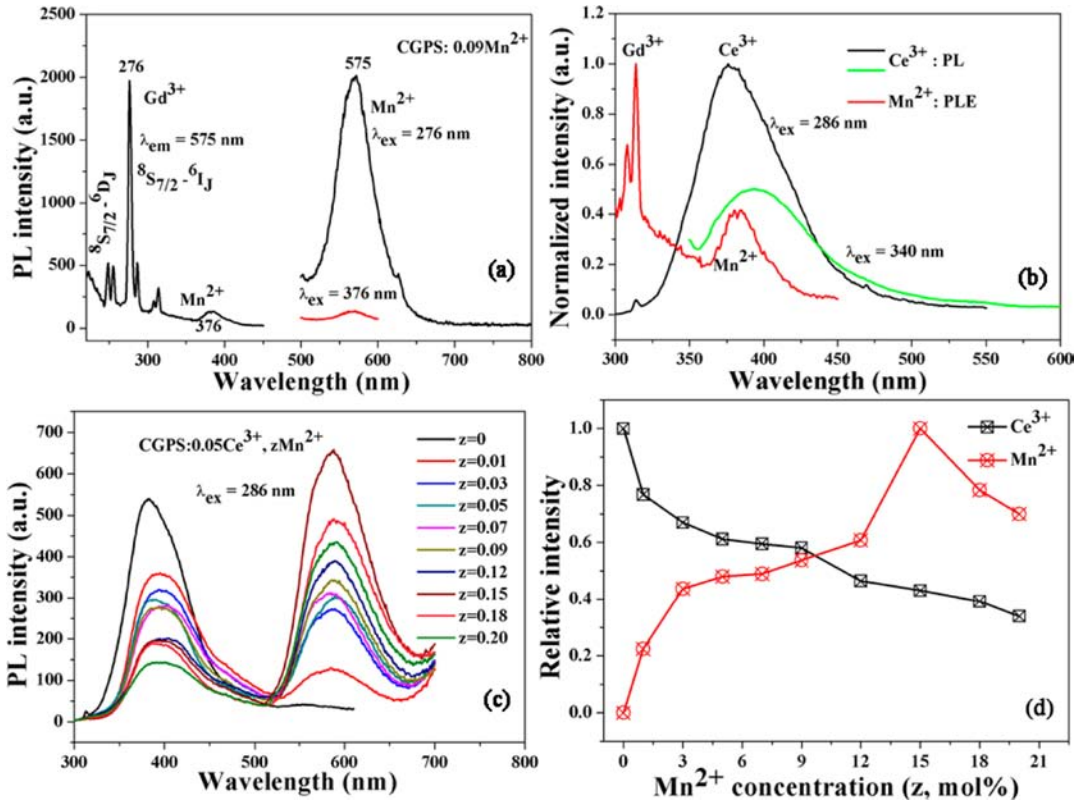

Figure 7. (a) Excitation and emission spectra of the CGPS:0.09Mn^{2+} sample. (b) Spectral overlap between the PL spectrum of CGPS:0.05Ce^{3+} (black or green solid lines) and the PLE spectrum of CGPS:0.09Mn^{2+} (red line). Variation of (c) the PL spectra and (d) the emission intensity of Ce^{3+} and Mn^{2+} in the CGPS:Ce^{3+},Mn^{2+} system with changing Mn^{2+} and fixed Ce^{3+} doping concentration.

significant spectral overlap observed from Figure 7b. This type of energy transfer is common and has been reported in other Ce^{3+}- and Mn^{2+}-coactivated phosphors such as $Ca_3Sc_2Si_3O_{12}$:Ce^{3+}/Mn^{2+} and $Ca_9Y(PO_4)_7$:Ce^{3+}/Mn^{2+}.[24,43] The excitation spectrum monitoring with the $Mn^{2+4}T_1 \rightarrow {}^6A_1$ transition (575 nm) of the CGPS:0.05Ce^{3+},0.09Mn^{2+} sample (Figure S5 in the SI) consists of excitation bands of the Ce^{3+} ion. The broad band (250−350 nm) is caused by a Ce^{3+} 4f → 5d transition. The presence of the Ce^{3+} absorption band suggests that the energy transfer process from Ce^{3+} to Mn^{2+} exists. In order to validate the occurrence of Ce^{3+} to Mn^{2+} energy transfer and determine the optimal Mn^{2+} doping concentration in CGPS:0.05Ce^{3+},zMn^{2+}, concentration-dependent luminescence measurements were performed. As revealed in Figure 7c,d, the emission intensity of Ce^{3+} decreases with increasing Mn^{2+} concentration, while the emission intensity of Mn^{2+} first increases with an increase of its concentration (z), reaching a maximum value at z = 0.15, and then decreases with a further increase (z) due to the concentration quenching effect. All of these results can validate the efficient energy transfer from Ce^{3+} to Mn^{2+}.

To further elucidate the energy-transfer process, we measured the Ce^{3+} decay curves and then calculated the lifetimes as well as energy-transfer efficiencies. As described by Blasse,[33] the decay behavior of Ce^{3+} can be expressed as

$$I = I_0 \exp(-t/\tau) \quad (5)$$

where I and I_0 are the luminescence intensities at time t and 0 and τ is the luminescence lifetime. Figure 8a shows the decay curves of Ce^{3+} emission in CGPS:0.05Ce^{3+},zMn^{2+} (z = 0.01, 0.03, and 0.05) under excitation at 286 nm, monitored at 380 nm. The average decay times were calculated as 24.57, 22.48, and 17.76 ns for CGPS:0.05Ce^{3+},zMn^{2+} with z = 0.01, 0.03, and 0.05, respectively. It can be seen that the decay lifetime of Ce^{3+} ions decreases with increasing Mn^{2+} concentration, which strongly supports energy transfer from the Ce^{3+} to Mn^{2+} ions, as reported by Zhang et al., Liu et al., and Huang et al.[24,43,46] η_T, the energy-transfer efficiency from Ce^{3+} to Mn^{2+} in CGPS:0.05Ce^{3+},zMn^{2+}, calculated by using eq 2 as a function of z under 286 and 340 nm UV excitation, is shown in Figure 8b. The energy-transfer efficiency was found to increase gradually from z = 0 to 0.20 with an increase of the Mn^{2+} concentration. The maximum energy-transfer efficiency can reach 67% and 70% when using 286 and 340 nm UV as the monitoring wavelength, respectively. All of the above results can elucidate that the energy-transfer efficiency from Ce^{3+} to Mn^{2+} is efficient. Figure 5 illustrates the energy-transfer mechanism for $Ce^{3+} \rightarrow Mn^{2+}$ in the CGPS host: Ce^{3+} ions can strongly absorb UV light from the ground state ($^2F_{5/2}$) to the excited state and then efficiently transfer the energy to the $^4T_1$ level of Mn^{2+} ions; subsequently, the $^4T_1$ level gives its characteristic transitions.

The critical distance (R_C) of energy transfer between the Ce^{3+} and Mn^{2+} ions calculated by the concentration quenching method (eq 1) is 9.71 Å. According to eq 4, when n = 8, the $I_{S0}/I_S - C_{Ce+Mn}^{n/3}$ plots show a linear relationship, which strongly indicates that energy transfer from Ce^{3+} to Mn^{2+} ions also has the dipole−quadrupole mechanism, as shown in Figure S6 in the SI. Considering dipole−quadrupole interaction, the critical distance from the sensitizer to the acceptor can also be calculated by the spectral overlap method, as expressed as follows:[20,43]

dx.doi.org/10.1021/ic3015578 | Inorg. Chem. 2012, 51, 11655−11664

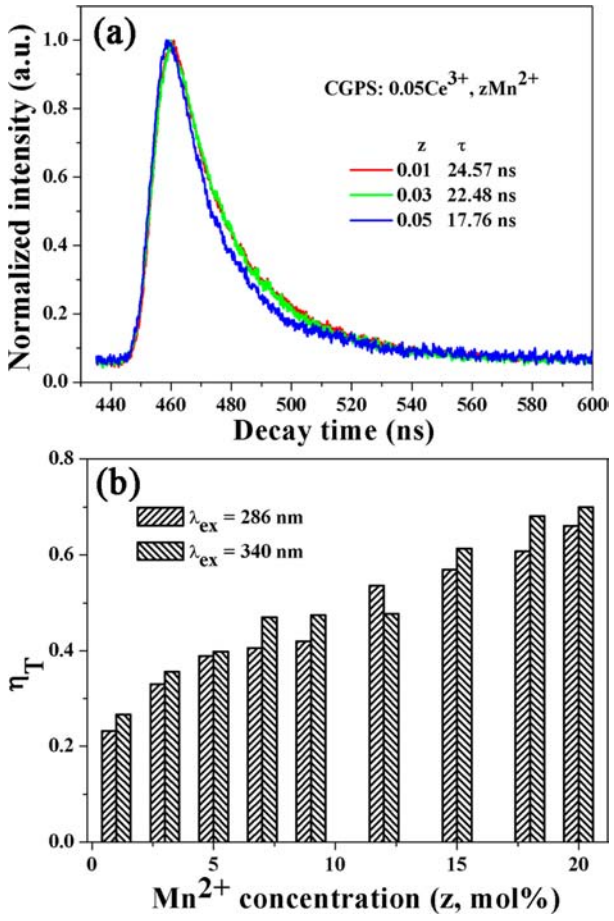

Figure 8. (a) Decay curves of Ce^{3+} emission in CGPS:0.05Ce^{3+},zMn^{2+} (z = 0.01, 0.03, and 0.05) under excitation at 286 nm, monitored at 380 nm. (b) Relationship of η_T versus Mn^{2+} ion concentration (λ_{ex} = 286 or 340 nm).

$$R_C^{\,8} = 3.024 \times 10^{12} \lambda_S^{\,2} f_q \int \frac{F_S(E)\, F_A(E)\, dE}{E^4} \qquad (6)$$

where f_q (=10^{-10}) is the oscillator strength of the involved absorption transition of the acceptor (Mn^{2+}), λ_S (in Å) is the wavelength position of the sensitizer's emission, E is the energy involved in the transfer (in eV), and $\int[F_S(E)\, F_A(E)\, dE]/E^4$ represents the spectral overlap between the normalized shapes of the Ce^{3+} emission $F_S(E)$ and the Mn^{2+} excitation $F_A(E)$, and in our case, it is calculated to be about 0.01153 eV^{-4}. Using eq 6, the critical distance R_C was estimated to be 9.15 Å. This result is in good agreement with that obtained from the concentration quenching method, which further reveals that the mechanism of energy transfer from the Ce^{3+} to Mn^{2+} ions is mainly due to dipole−quadrupole interaction.

Energy transfer makes it possible to obtain both the blue emission of the Ce^{3+} ions and the yellow emission of the Mn^{2+} ions in a single host, which is a feasible route to realizing color-tunable emission under excitation of UV light.[20] This result is also confirmed by their CIE chromaticity coordinates shown in Table 2. We can find that the color tone of the phosphors shifts gradually from blue to white and eventually to yellow with an increase of the doping content of Mn^{2+}, confirming that the CIE chromaticity coordinates are tunable. Especially, a wide-ranged white emission can be obtained by precise control of the content of the Mn^{2+} ions between 0.01 and 0.03. Hence, this material could meet the needs of different illumination applications.

3.4. CL Properties of CGPS:Ce^{3+}/Tb^{3+}/Mn^{2+}. In order to explore the potential application of the as-prepared CGPS:Ce^{3+}/Tb^{3+}/Mn^{2+} phosphors in FEDs, their CL properties are investigated in detail. Under low-voltage electron-beam excitation (accelerating voltage = 4 kV; filament current = 86 mA), when Ce^{3+} and Tb^{3+} are codoped into the CGPS host, maintaining the Ce^{3+} concentration at 0.05 and changing the Tb^{3+} concentration from 0 to 0.20, the CL intensity of Ce^{3+} gradually decreases and the CL intensity of Tb^{3+} gradually increases with an increase of the Tb^{3+} concentration. CGPS:0.05Ce^{3+},0.15Tb^{3+} could show green emission, as shown in the inset of Figure 9, which could also be confirmed

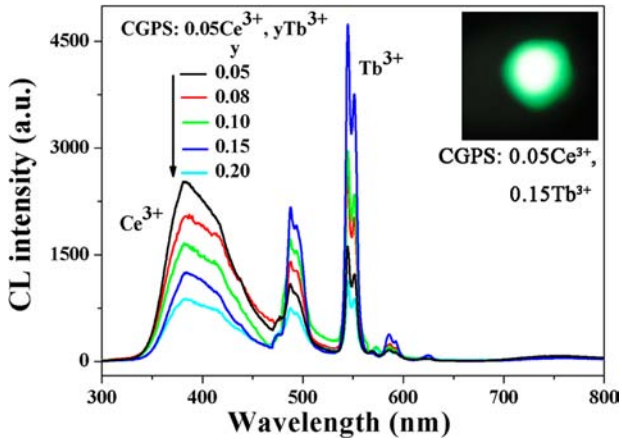

Figure 9. CL spectra of CGPS:0.05Ce^{3+},yTb^{3+}. The insets show the digital cathodoluminescence photographs of the CGPS:0.05Ce^{3+},0.15Tb^{3+} samples (accelerating voltage = 4.0 kV; filament current = 86 mA).

by their CIE coordinates (0.261, 0.543). Besides, the CIE chromaticity coordinate information of the rest of the samples is shown in Figure 10. As shown in Figure 11, the CL spectra of CGPS:Ce^{3+}/Mn^{2+} samples are similar to their PL spectra,

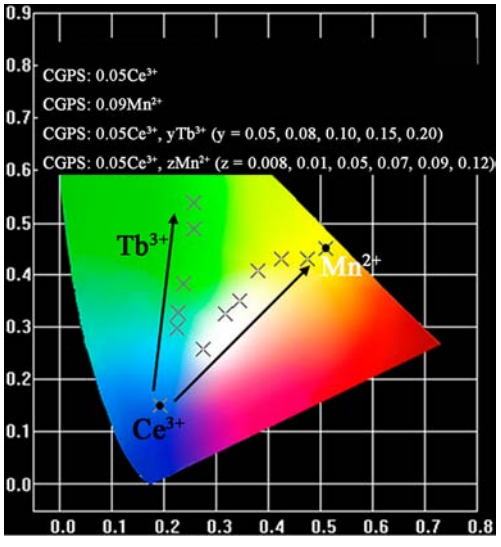

Figure 10. CIE chromaticity coordinates (x, y) of CGPS:Ce^{3+}/Tb^{3+}/Mn^{2+} samples under low-voltage electron-beam excitation (accelerating voltage = 4.0 kV; filament current = 86 mA).

dx.doi.org/10.1021/ic3015578 | Inorg. Chem. 2012, 51, 11655−11664

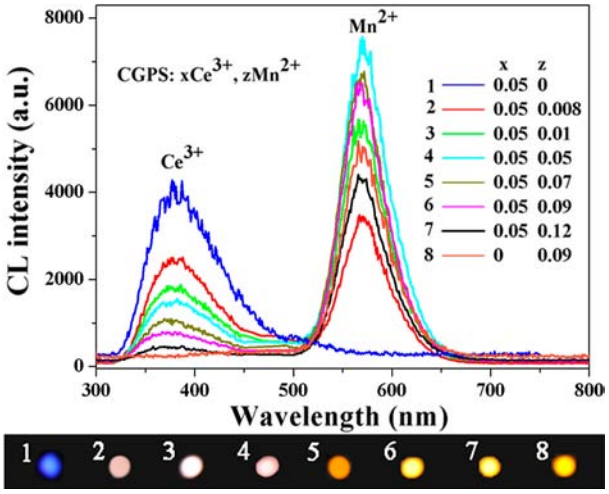

Figure 11. CL spectra of CGPS:xCe^{3+},zMn^{2+}. The insets show the digital cathodoluminescence photographs of CGPS:xCe^{3+},zMn^{2+} samples (1) x = 0.05, z = 0, (2) x = 0.05, z = 0.008, (3) x = 0.05, z = 0.01, (4) x = 0.05, z = 0.05, (5) x = 0.05, z = 0.07, (6) x = 0.05, z = 0.09, (7) x = 0.05, z = 0.12, and (8) x = 0, z = 0.09 (accelerating voltage = 4.0 kV; filament current = 86 mA).

which give the characteristic transitions of Ce^{3+} and Mn^{2+}, respectively. The insets 1−8 show digital CL photographs of the CGPS:xCe^{3+},zMn^{2+} samples. The CGPS:0.05Ce^{3+} and CGPS:0.09Mn^{2+} samples emit blue and yellow light under low-voltage electron-beam excitation, respectively, which can also be determined by their CIE coordinates (0.192, 0.150) or (0.511, 0.450) for pure Ce^{3+}- or Mn^{2+}-activated phosphors, respectively. It is possible to obtain white light in the CGPS host by codoping with Ce^{3+} and Mn^{2+} and appropriately adjusting their concentrations. In our experiments, we fixed the Ce^{3+} concentration at 0.05 and changed the Mn^{2+} ion concentration from 0.008 to 0.12. As is shown in Figure 11, the CL intensity of Ce^{3+} gradually decreases and the CL emission intensity of Mn^{2+} gradually increases with an increase of the Mn^{2+} concentration. According to our experiment, when z = 0.01, the blue and yellow emissions have comparable intensity, which results in a bright-white emission, as shown in the inset 3 (Figure 11). The CIE coordinates of CGPS:0.05Ce^{3+},0.01Mn^{2+} (0.322, 0.326) are close to those of the standard white light (0.33, 0.33).

CGPS:0.05Ce^{3+}, CGPS:0.05Ce^{3+},0.10Tb^{3+}, CGPS:0.05Ce^{3+},0.01Mn^{2+}, and CGPS:0.05Ce^{3+},0.05Mn^{2+} phosphors have been investigated as a function of the accelerating voltage and filament current. When the accelerating voltage is fixed at 5 kV, the CL intensity increases upon an increase in the filament current from 82 to 90 mA (Figure 12a). Similarly, under a 92 mA filament current, the CL intensity also increases upon an increase in the the accelerating voltage from 2 to 6 kV (Figure 12b). The increases in the CL brightness with increases in the electron energy and filament current are attributed to the deeper penetration of the electrons into the phosphor body and the larger electron-beam current density. According to the empirical formula

$$L\ [\text{Å}] = 250\left(\frac{A}{\rho}\right)\left(\frac{E}{\sqrt{Z}}\right)^{n}, \quad n = \frac{1.2}{1 - 0.29 \log Z} \qquad (7)$$

where A is the atomic or molecular weight of the material, ρ is the bulk density, Z is the atomic number or the number of

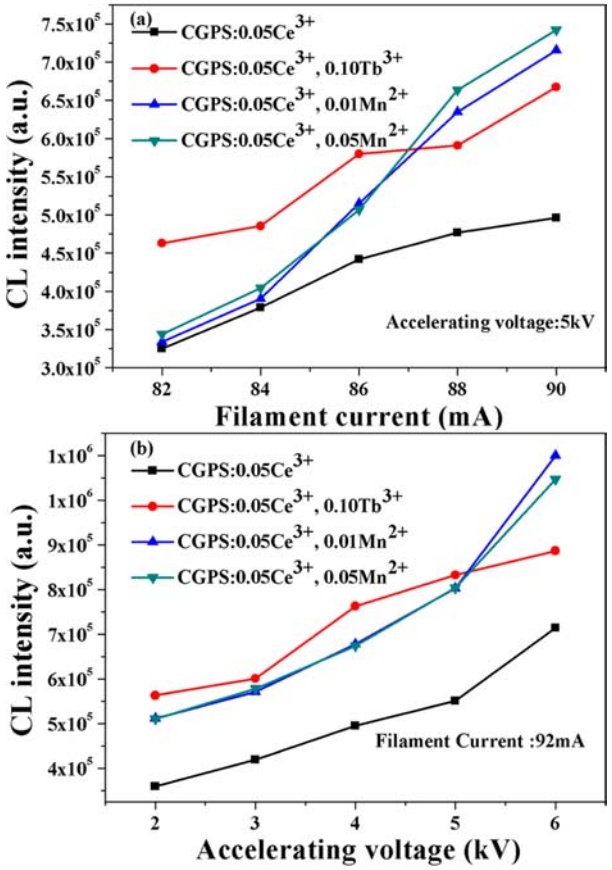

Figure 12. CL intensities of CGPS:0.05Ce^{3+}, CGPS:0.05Ce^{3+},0.10Tb^{3+}, CGPS:0.05Ce^{3+},0.01Mn^{2+}, and CGPS:0.05Ce^{3+},0.05Mn^{2+} samples as a function of (a) the filament current and (b) accelerating voltage.

electrons per molecule in the compounds, and E is the accelerating voltage (kV).[20,47] For CGPS:0.05Ce^{3+},0.01Mn^{2+}, Z = 801, A = 1808.4, and ρ = 5.31 g cm^{-3}; the estimated electron penetration depths at 4, 5, and 6 kV are about 3, 16, and 64 nm, respectively. For CL, the Ce^{3+}, Tb^{3+}, and Mn^{2+} ions are excited by the plasma produced by the incident electrons. The deeper the electron penetration depth, the more plasma will be produced, which results in more Ce^{3+}, Tb^{3+}, and Mn^{2+} ions being excited, and thus the CL intensity increases.[40] The stability for the phosphor is very important for FED application. Thus, we also investigated the degradation behavior of CGPS:Ce^{3+},Mn^{2+} samples under low-voltage electron-beam excitation. Figure 13 (green line) shows the decay behavior of the CL intensity of a representative CGPS:0.05Ce^{3+},0.01Mn^{2+} sample under continuous electron bombardment when accelerating voltage = 5.0 kV and filament current = 90 mA. The CL peak positions are almost the same as those before electron bombardment. However, the CL intensity of the studied sample monotonously decreases with a prolonging of the electron bombardment time. After continuous electron radiation for 2 h, the CL intensities of the CGPS:0.05Ce^{3+},0.01Mn^{2+} sample fall to 82% of the initial value. The accretion of graphitic carbon during electron-beam exposure at high current densities is a well-known effect, and this carbon contamination will prevent low-energy electrons from reaching the phosphor grains and also exacerbate surface charging and thus lower the CL efficiency.[20,48] In addition, after stopping bombardment for a while the CL intensity could not

dx.doi.org/10.1021/ic3015578 | Inorg. Chem. 2012, 51, 11655−11664

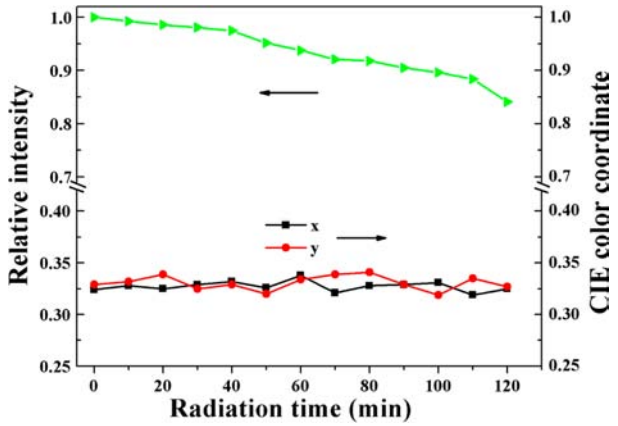

Figure 13. Dependence of the relative CL intensity and CIE color coordinates of a representative CGPS:0.05Ce^{3+},0.01Mn^{2+} sample on the radiation time under electron-beam excitation (accelerating voltage = 5.0 kV; filament current = 90 mA).

restore to the initial value, indicating permanent damage to the phosphor occurs, which is another reason for the decrease of the CL intensity. On the other hand, the CIE chromaticity coordinates of the CGPS:0.05Ce^{3+},0.01Mn^{2+} sample are nearly invariable under continuous electron radiation for 2 h, as presented in Figure 13. In summary, the short-time experiment (2 h) indicates that the stability of the CL intensity and CIE color coordinates of the as-prepared CGPS:0.05Ce^{3+},0.01Mn^{2+} samples are good, which shows potential application in the FEDs.

4. CONCLUSION

A single-phased, color-tunable-emitting phosphor CGPS has been prepared by a conventional solid-state reaction. The energy transfer from Ce^{3+} to Tb^{3+}/Mn^{2+} in the CGPS host has been studied in detail. The energy transfer from Ce^{3+} to Mn^{2+} in CGPS phosphors has been demonstrated to be a resonant type via a dipole−quadrupole mechanism, and the critical distance (R_C) for Ce^{3+} to Mn^{2+} calculated by the concentration quenching and spectral overlap methods are 9.71 and 9.15 Å, respectively. A color-tunable emission in CGPS:Ce^{3+}/Tb^{3+}/Mn^{2+} phosphors can be realized by the Ce^{3+} → Tb^{3+} or Ce^{3+} → Mn^{2+} energy transfer. White CL has been realized in a single-phased CGPS host by codoping with Ce^{3+} and Mn^{2+} for the first time. It is worth noting that the CGPS:Ce^{3+}/Tb^{3+}/Mn^{2+} phosphors have superior stability under electron bombardment. Because of their strong CL intensity, good CIE chromaticity, stability, and low raw material cost, these phosphors have potential applications in FEDs.

■ ASSOCIATED CONTENT

Supporting Information

XRD patterns of the CGPS host and different Ce^{3+}-doped CGPS samples (Figure S1); XRD patterns of the CGPS host and different Ce^{3+}/Mn^{2+}/Tb^{3+}-doped CGPS samples (Figure S2); crystal structure of CGPS host (Figure S3); excitation spectra of CGPS:0.05Ce^{3+}/0.15Tb^{3+} monitored at 380 and 545 nm (Figure S4); excitation spectra of CGPS:0.05Ce^{3+}/0.09Mn^{2+} monitored at 380 and 575 nm (Figure S5); dependence of I_{S0}/I_S of Ce^{3+} on (a) $C_{Ce+Mn}^{6/3}$, (b) $C_{Ce+Mn}^{8/3}$, and (c) $C_{Ce+Mn}^{10/3}$ (Figure S6). This material is available free of charge via the Internet at http://pubs.acs.org.

■ AUTHOR INFORMATION

Corresponding Author

*E-mail: jlin@ciac.jl.cn.

Notes

The authors declare no competing financial interest.

■ ACKNOWLEDGMENTS

This project is financially supported by National Basic Research Program of China (Grant 2010CB327704) and the National Natural Science Foundation of China (NSFC Grants 51172227, 51272248, and 20921002) and funds from Guangdong Province (2011A090100011).

■ REFERENCES

(1) Höppe, H. A. *Angew. Chem., Int. Ed.* **2009**, *48*, 3572−3582.
(2) Justel, T.; Krupa, J. C.; Wiechert, D. U. *J. Lumin.* **2001**, *93*, 179−189.
(3) Xie, R. J.; Hirosaki, N.; Sakuma, K.; Yamamoto, Y.; Mitomo, M. *Appl. Phys. Lett.* **2004**, *84*, 5404−5406.
(4) Kim, C. H.; Kwon, I. E.; Park, C. H.; Hwang, Y. J.; Bae, H. S.; Yu, B. Y.; Pyun, C. H.; Hong, G. Y. *J. Alloys Compd.* **2000**, *311*, 33−39.
(5) Psuja, P.; Hreniak, D.; Strek, W. *J. Nanomater.* **2007**, *2007*, 81350.
(6) Dai, Q.; Foley, M. E.; Breshike, C. J.; Lita, A.; Strouse, G. F. *J. Am. Chem. Soc.* **2011**, *133*, 15475−15486.
(7) Wakefield, G.; Holland, E.; Dobson, P. J.; Hutchison, J. L. *Adv. Mater.* **2001**, *13*, 1557−1560.
(8) Mao, Y.; Tran, T.; Guo, X.; Huang, J. Y.; Shih, C. K.; Wang, K. L.; Chang, J. P. *Adv. Funct. Mater.* **2009**, *19*, 748−754.
(9) Dhanaraj, J.; Jagannathan, R.; Trivedi, D. C. *J. Mater. Chem.* **2003**, *13*, 1778−1782.
(10) Yang, S.; Stoffers, C.; Zhang, F.; Jacobsen, S. M.; Wagner, B. K.; Summers, C. J.; Yocom, N. *Appl. Phys. Lett.* **1998**, *72*, 158−160.
(11) Zhang, F. L.; Yang, S.; Stoffers, C.; Penczek, J.; Yocom, P. N.; Zaremba, D.; Wagner, B. K.; Summers, C. J. *Appl. Phys. Lett.* **1998**, *72*, 2226−2228.
(12) Li, Y. C.; Chang, Y. H.; Lin, Y. F.; Lin, Y. J.; Chang, Y. S. *Appl. Phys. Lett.* **2006**, *89*, 081110.
(13) Rao, B. V.; Nien, Y. T.; Hwang, W. S.; Chen, I. G. *J. Electrochem. Soc.* **2009**, *156*, J338−J341.
(14) Gundiah, G.; Shimomura, Y.; Kijima, N.; Cheetham, A. K. *Chem. Phys. Lett.* **2008**, *455*, 279−283.
(15) Geng, D.; Li, G.; Shang, M.; Peng, C.; Zhang, Y.; Cheng, Z.; Lin, J. *Dalton Trans.* **2012**, *41*, 3078−3086.
(16) Tang, Y. S.; Hu, S. F.; Lin, C. C.; Bagkar, N. C.; Liu, R. S. *Appl. Phys. Lett.* **2007**, *90*, 151108.
(17) Feldmann, C.; Justel, T.; Ronda, C. R.; Schmidt, P. J. *Adv. Funct. Mater.* **2003**, *13*, 511−516.
(18) Guo, N.; Song, Y.; You, H.; Jia, G.; Yang, M.; Liu, K.; Zheng, Y.; Huang, Y.; Zhang, H. *Eur. J. Inorg. Chem.* **2010**, 4636−4642.
(19) Huang, C. H.; Chen, T. M.; Liu, W. R.; Chiu, Y. C.; Yeh, Y. T.; Jang, S. M. *ACS Appl. Mater. Interfaces* **2010**, *2*, 259−264.
(20) Li, G.; Geng, D.; Shang, M.; Peng, C.; Cheng, Z.; Lin, J. *J. Mater. Chem.* **2011**, *21*, 13334−13344.
(21) Blasse, G.; Bril, A. *J. Chem. Phys.* **1967**, *47*, 5139−5145.
(22) Shang, M.; Li, G.; Kang, X.; Yang, D.; Geng, D.; Lin, J. *ACS Appl. Mater. Interfaces* **2011**, *3*, 2738−2746.
(23) Blasse, G.; Bril, A. *J. Chem. Phys.* **1967**, *47*, 1920−1926.
(24) Liu, Y.; Zhang, X.; Hao, Z.; Wang, X.; Zhang, J. *Chem. Commun.* **2011**, *47*, 10677−10679.
(25) Li, G.; Zhang, Y.; Geng, D.; Shang, M.; Peng, C.; Cheng, Z.; Lin, J. *ACS Appl. Mater. Interfaces* **2012**, *4*, 296−305.
(26) Zhang, J.; Liang, H.; Su, Q. *J. Phys. D: Appl. Phys.* **2009**, *42*, 105110.
(27) Boyer, L.; Carpena, J.; Lacout, J. L. *Solid State Ionics* **1997**, *95*, 121−129.
(28) Zhu, G.; Wang, Y.; Ci, Z.; Liu, B.; Shi, Y.; Xin, S. *J. Electrochem. Soc.* **2011**, *158*, J236−J242.

(29) El Ouenzerfi, R.; Panczer, G.; Goutaudier, C.; Cohen-Adad, M. T.; Boulon, G.; Trabelsi-Ayedi, M.; Kbir-Ariguib, N. *Opt. Mater.* **2001**, *16*, 301−310.
(30) Zhao, D.; Li, L.; Davis, L. L.; Weber, W. J.; Ewing, R. C. *Gadolinium Borosilicate Glass-Bonded Gd-Silicate Apatite: A Glass−Ceramic Nuclear Waste Form for Actinides*; Cambridge University Press: Cambridge, U.K., 2001; Vol. *663*, pp 199−206.
(31) Blasse, G. *J. Solid State Chem.* **1975**, *14*, 181−184.
(32) Lin, J.; Su, Q. *J. Alloys Compd.* **1994**, *210*, 159−163.
(33) Blasse, G.; Grabmaier, B. *Luminescent materials*; Springer-Verlag: Berlin, 1994; Chapters 4 and 5.
(34) Shannon, R. D. *Acta Crystallogr., Sect. A* **1976**, *32*, 751−767.
(35) Lin, J.; Su, Q. *J. Mater. Chem.* **1995**, *5*, 1151−1154.
(36) Dexter, D. L.; Schulman, J. H. *J. Chem. Phys.* **1954**, *22*, 1063−1070.
(37) Chan, T. S.; Lin, C. C.; Liu, R. S.; Xie, R. J.; Hirosaki, N.; Cheng, B. M. *J. Electrochem. Soc.* **2009**, *156*, J189−J191.
(38) Blasse, G. *Philips Res. Rep.* **1969**, *24*, 131−144.
(39) Tian, Z.; Liang, H.; Han, B.; Su, Q.; Tao, Y.; Zhang, G.; Fu, Y. *J. Phys. Chem. C* **2008**, *112*, 12524−12529.
(40) Geng, D.; Li, G.; Shang, M.; Yang, D.; Zhang, Y.; Cheng, Z.; Lin, J. *J. Mater. Chem.* **2012**, *22*, 14262−14271.
(41) Yang, W. J.; Chen, T. M. *Appl. Phys. Lett.* **2006**, *88*, 101903.
(42) Reisfeld, R.; Boehm, L. *J. Solid State Chem.* **1972**, *4*, 417−424.
(43) Huang, C. H.; Kuo, T. W.; Chen, T. M. *ACS Appl. Mater. Interfaces* **2010**, *2*, 1395−1399.
(44) Yang, W. J.; Luo, L. Y.; Chen, T. M.; Wang, N. S. *Chem. Mater.* **2005**, *17*, 3883−3888.
(45) Lin, J.; Sanger, D. U.; Mennig, M.; Barner, K. *Thin Solid Films* **2000**, *360*, 39−45.
(46) Zhang, C.; Huang, S.; Yang, D.; Kang, X.; Shang, M.; Peng, C.; Lin, J. *J. Mater. Chem.* **2010**, *20*, 6674−6680.
(47) Feldman, C. *Phys. Rev.* **1960**, *117*, 455−459.
(48) Duan, C. Y.; Chen, J.; Deng, S. Z.; Xu, N. S.; Zhang, J. H.; Liang, H. B.; Su, Q. *J. Vac. Sci. Technol. B* **2007**, *25*, 618−622.